

Quantum Monte Carlo method for the ground state of many-boson systems

Wirawan Purwanto and Shiwei Zhang^y

Department of Physics, The College of William and Mary, Williamsburg, Virginia 23187

(Dated: April 17, 2024)

We formulate a quantum Monte Carlo (QMC) method for calculating the ground state of many-boson systems. The method is based on a field-theoretical approach, and is closely related to existing fermion auxiliary-field QMC methods which are applied in several fields of physics. The ground-state projection is implemented as a branching random walk in the space of permanents consisting of identical single-particle orbitals. Any single-particle basis can be used, and the method is in principle exact. We illustrate this method with a trapped atomic boson gas, where the atoms interact via an attractive or repulsive contact two-body potential. We choose as the single-particle basis a real-space grid. We compare with exact results in small systems, and arbitrarily-sized systems of untrapped bosons with attractive interactions in one dimension, where analytical solutions exist. We also compare with the corresponding Gross-Pitaevskii (GP) mean-field calculations for trapped atoms, and discuss the close formal relation between our method and the GP approach. Our method provides a way to systematically improve upon GP while using the same framework, capturing interaction and correlation effects with a stochastic, coherent ensemble of non-interacting solutions. We discuss various algorithmic issues, including importance sampling and the back-propagation technique for computing observables, and illustrate them with numerical studies. We show results for systems with up to $N = 400$ bosons.

I. INTRODUCTION

The study of many-body quantum systems has been a very challenging research field for many years. Computational methods have often been the way of choice to extract theoretical understanding on such systems. Most computational quantum mechanical studies are based on simpler mean-field theories such as the Gross-Pitaevskii (GP) equation for bosons or the Kohn-Sham density-functional theory (DFT) for fermions. Despite their remarkable success, the treatment of particle interaction or correlation effects is only approximate within these approaches, and can lead to incorrect results, especially as the strength of particle interactions is increased. It is therefore necessary to develop alternative computational methods that can describe the effect of interaction more accurately and reliably.

In this paper we present a quantum Monte Carlo (QMC) method to study the ground state of many-boson systems. The method is in principle exact. Our interest in the development and use of this method was motivated by the realization of the Bose-Einstein condensation in ultracold atomic gases [1]. These are dilute gases consisting of interacting alkali atoms. The interaction among the atoms is well described by a simple two-body potential, either attractive or repulsive, based on the scattering length. For weakly-interacting systems the mean-field GP approach has, as expected, performed extremely well [2, 3]. More recently, Feshbach resonances [4] have successfully been used as a powerful way to tune the strength of the interaction experimentally. This provides a source of rich physics, and increases the need for theoretical methods which can benchmark GP and provide an alternative where GP is inadequate.

Several QMC methods exist for calculating the properties

of interacting many-body systems. The ground-state diffusion Monte Carlo [5] and the finite-temperature path-integral Monte Carlo (PIMC) [6] methods, which work in many-particle configuration space and in the first-quantized framework, have been successfully applied to a variety of boson and fermion systems. In the context of atomic gases, Krauth [7], Gruter *et al.* [8], and Holzmann and Krauth [9] have employed PIMC to study finite-temperature properties of trapped bosons with positive scattering lengths, modeling the two-body interactions by a hard-sphere potential. Glyde and co-workers have studied the ground state of trapped bosons, also by hard spheres [10, 11]. Ulmke and Scalapin [12] did finite-temperature QMC calculations on quantum spin systems and the Bose-Hubbard model. In the latter calculation, a hard-core repulsive potential was assumed, which allowed a transformation of the problem into an XXZ spin-like problem that can be treated with a fermion QMC method.

Our method is based on the auxiliary field quantum Monte Carlo (AFQMC) approach [13, 14]. The AFQMC is a field-theoretical method, where many-body propagators resulting from two-body interactions are transformed, by use of auxiliary fields, into a many-dimensional integral over one-body propagators [15, 16]. The many-dimensional integral is then computed using stochastic means. The AFQMC framework is appealing for several reasons. Working in second-quantization, it automatically imposes the proper particle-permutation symmetry or antisymmetry. It provides a many-body method with close formal relation to mean-field approaches, as we discuss later. In addition, it allows convenient calculation of the observables and correlation functions.

The AFQMC method has been widely employed to study fermion systems in condensed matter [17, 18, 19], nuclear physics [20, 21], and lattice gauge theory. In this paper, we generalize the fermion ground-state auxiliary-field quantum Monte Carlo method [19, 22] to many-boson systems. We project the many-body boson ground-state from an initial trial state $|\psi_T\rangle$. Our choice of $|\psi_T\rangle$ is a permanent consisting of N identical single-particle orbitals, which was first suggested in

Electronic address: wirawan@camelot.physics.wm.edu

^yElectronic address: shiwei@physics.wm.edu

a model calculation by Sugiyama and Koonin [14]. The many-body ground state is projected from $|\psi_T\rangle$ with open-ended, branching random walks to sample the auxiliary fields. We formulate an importance sampling scheme, which greatly improves the efficiency of the method and makes possible simulations of large systems. We also discuss in detail the back-propagation technique which allows convenient calculation of virtually any ground-state observables.

Our method retains all the advantages of AFQMC. It allows the use of any single-particle basis, which in this paper is chosen to be a real-space grid. As we discuss in Sec. VI, it provides a means for true many-body calculations in a framework which closely relates to the GP approach. The approach can be viewed as a stochastic collection of parallel GP-like calculations whose “coherent” linear combination gives the interaction and correlation effects.

In this paper we present our QMC method for bosons and discuss its behavior and characteristics. We use a trapped atomic boson gas as our test system, where the atoms interact via an attractive or repulsive contact two-body potential. A sufficiently detailed description of the method is given to facilitate implementation. Compared to its fermionic counterpart, our method here is formally simpler. It therefore also offers opportunities to study algorithmic issues. Because of the intense interest in methods for treating correlated systems (fermions or bosons) and the relatively early stage of this type of QMC methods, a second purpose of the paper is to use the bosonic test ground to explore, discuss, and illustrate the generic features of ground-state QMC methods based on auxiliary fields. An example is the case of repulsive interactions, where a phase problem appears in a bosonic system, which provides a clean test ground to study methods for controlling this problem [22], which is crucial for applications in fermion systems. The majority of the applications in this paper will be to systems where exact results are available for benchmark. These include small systems, which can be diagonalized exactly, and the case of untrapped bosons with attractive interactions in one dimension, where analytical solutions exist. It is worth emphasizing that the method scales gracefully (similar to GP) and allows calculations for a large number (N) of bosons. We will show results for larger systems ($N = 1000$ sites and hundreds of particles) in one- and three-dimensions to illustrate this.

Our paper is organized as follows. In section II, we establish some conventions and review the basic ground-state projection and auxiliary-field quantum Monte Carlo method. In section III, we introduce our new AFQMC implementation for bosons, including the formulation of an importance-sampling scheme and the back-propagation technique for convenient calculation of virtually any ground-state observables. In section IV, we describe the implementation of our method to study the ground state of a trapped Bose atomic gas, which we model by a Bose-Hubbard Hamiltonian with an external trapping potential. We also describe our implementation of the GP approach to study the same Hamiltonian. In section V, we present our computational results. We benchmark the method in systems where exact results are available. We also provide examples to illustrate the behavior and key charac-

teristics of our method. We carry out GP calculations on the same Hamiltonian and compare the results with those from our QMC calculations. In section VI we comment on some characteristics of the method, further discuss its relation to and differences from GP, and mention future directions and some immediate applications of this method. Some computing issues will also be discussed. Finally, in the appendices we provide additional technical details of the method.

II. BACKGROUND

A. Many-body Hamiltonian

We use the second quantized formalism throughout this paper. We assume that an appropriate set of single-particle basis $\{|\phi_i\rangle\}$ has been chosen, in terms of which the wave functions will be expanded. For simplicity, we assume that the single-particle basis is orthonormal, although this is not required. The number of basis states is M . The operators c_i^\dagger and c_i , respectively, are the usual creation and annihilation operator for the state $|\phi_i\rangle$. They satisfy the commutation relation $[c_i, c_j^\dagger] = \delta_{ij}$. This automatically imposes the symmetrization requirement of the many-body wave functions.

We limit our discussion to a quantum-mechanical, many-body system with two-body interactions. The Hamiltonian \hat{H} has a general form of

$$\hat{H} = \hat{K} + \hat{V}; \quad (1)$$

where \hat{K} is the sum total of all the one-body operators (the kinetic energy and external potential energy),

$$\hat{K} = \sum_{ij} K_{ij} c_i^\dagger c_j;$$

and \hat{V} contains the two-body interactions:

$$\hat{V} = \sum_{ijkl} V_{ijkl} c_i^\dagger c_j^\dagger c_k c_l;$$

Our objective is to calculate the ground state properties of such a system, which contains a fixed number of particles, N .

B. Ground state projection

The ground state wave function $|\psi_0\rangle$ can be readily extracted from a given trial solution $|\psi_T\rangle$ using the ground-state projection operator

$$P_{gs} = e^{-\hat{H} E_T} e^{\hat{H} E_T}; \quad (2)$$

where E_T is the best guess of the ground-state energy, provided that $|\psi_T\rangle$ is not orthogonal to $|\psi_0\rangle$. Applying the operator P_{gs} repeatedly to the initial wave function $|\psi_T\rangle$ would

exponentially attenuate the excited-state components of the initial wave function, leaving only the ground state:

$$(P_{gs})^n |j\rangle_T \xrightarrow{n \rightarrow \infty} |j_0\rangle; \quad (3a)$$

$$P_{gs} |j_0\rangle \xrightarrow{n \rightarrow \infty} |j_0\rangle; \quad (3b)$$

Because of its resemblance to the real-time propagator, the operator P_{gs} is also called the imaginary-time propagator. In ground-state QMC methods, P_{gs} is evaluated by means of a Monte Carlo sampling, resulting in a stochastic representation of the ground-state wave function.

C. Basic auxiliary-field method

Two essential ingredients are needed in order to evaluate P_{gs} within a reasonable computing time. The first is the Trotter-Suzuki approximation [23, 24]. The propagator is broken up into a product of exponential operators, which becomes exact in the limit $\tau \rightarrow 0$. The second-order form of this approximation is

$$e^{-(\hat{K} + \hat{V})\tau} = e^{-\frac{\tau}{2}\hat{K}} e^{-\hat{V}\tau} e^{-\frac{\tau}{2}\hat{K}} + O(\tau^3); \quad (4)$$

The second ingredient is the Hubbard-Stratonovich (HS) transformation [15, 16], which allows us to reduce the two-body propagator to a multidimensional integral involving only one-body operators, using the following identity: [25]

$$e^{\frac{\tau}{2}\hat{V}^2} = \int \frac{1}{\mathcal{P}} \prod_i dx_i e^{\frac{\tau}{2}x_i^2} e^{x_i \hat{V}}; \quad (5)$$

where \hat{V} is a one-body operator:

$$\hat{V} = \sum_{ij} \hat{v}_{ij} c_i^\dagger c_j;$$

The hermiticity of \hat{V} allows us to decompose it into a sum of the square of one-body operators $\hat{v}_i g$ (see, for example, Refs. 19 and 25):

$$\hat{V} = \sum_i \frac{1}{2} \hat{v}_i^2; \quad (6)$$

Because of this, we can always apply the Hubbard-Stratonovich transformation on a general two-body potential operator:

$$\begin{aligned} e^{-\hat{V}\tau} &= e^{-\sum_i \frac{\tau}{2} \hat{v}_i^2} + O(\tau^2) \\ &= \int \prod_i \frac{1}{Z_i} \int_{-\infty}^{\infty} dx_i \frac{1}{\mathcal{P}} e^{\frac{\tau}{2}x_i^2} e^{x_i \hat{v}_i} + O(\tau^2); \end{aligned} \quad (7)$$

In general, the Trotter breakup incurs an additional systematic error of $O(\tau^2)$.

Applying these two procedures, we obtain an approximate expression of the ground-state projection operator:

$$P_{gs} = e^{-E_T \tau} e^{\frac{\tau}{2}\hat{K}} \left(\prod_i \int_{-\infty}^{\infty} dx_i \frac{1}{\mathcal{P}} e^{\frac{\tau}{2}x_i^2} e^{x_i \hat{v}_i} \right) e^{-\frac{\tau}{2}\hat{K}} + O(\tau^2); \quad (8)$$

where $p(\mathbf{x})$ is the normalized Gaussian probability density function with unit standard deviation: $p(\mathbf{x}) = \frac{1}{\mathcal{P}} e^{-\frac{1}{2}\mathbf{x}^2}$. This approach is applicable to both boson and fermion systems. It enables us to compute the exact ground state of a quantum many-body system. To reduce the systematic error from the finite timestep τ , the so-called ‘‘Trotter error’’, small timesteps are necessary. Often, calculations are performed for several τ values, then an extrapolation to $\tau \rightarrow 0$ is made to remove the Trotter error.

For convenience we define the following notations:

$\mathbf{x} = \{x_1, x_2, \dots, x_Q\}$: the collection of all the auxiliary-fields.

$p(\mathbf{x}) = \prod_i p(x_i)$: a (normalized) multidimensional probability density function, which is the product of the one-dimensional probability density functions $p(x_i)$.

$\hat{B}_v(\mathbf{x})$: a product of the exponential one-body operators arising from the auxiliary-field transformation. From Eq. (8), $\hat{B}_v(\mathbf{x}) = \prod_i e^{x_i \hat{v}_i}$.

$\hat{B}(\mathbf{x})$: the product of $\hat{B}_v(\mathbf{x})$ with all other one-body exponential operators that do not depend on the auxiliary fields \mathbf{x} , and all the necessary scalar prefactors. For the projector in Eq. (8), $\hat{B}(\mathbf{x}) = e^{-E_T \tau} e^{\frac{\tau}{2}\hat{K}} \hat{B}_v(\mathbf{x}) e^{-\frac{\tau}{2}\hat{K}}$.

With these notations, P_{gs} takes a generic form of a high-dimensional integral operator:

$$P_{gs} = \int d\mathbf{x} p(\mathbf{x}) \hat{B}(\mathbf{x}); \quad (9)$$

D. Wave function representation

We write our wave functions in terms of the basis functions j_i . A single-particle wave function is written as

$$j_i = \sum_i^X \phi_i^X, \quad j_i = \sum_i^X \phi_i^X, \quad j_i = \sum_i^X \phi_i^X, \quad j_i = \sum_i^X \phi_i^X. \quad (10)$$

A single-permanent, N -Bosons wave function is given by

$$j_i = \sum_1^Y \sum_2^Y \dots \sum_N^Y j_i. \quad (11)$$

In general, the exact ground state wave function is a superposition of such permanents. Unlike the fermionic case, where the particles occupy mutually orthogonal orbitals, there is no such restriction on the orbitals here. We use this freedom in our method to have all the bosons occupy the same orbital in j_i , which greatly simplifies the computation [14]. We will refer to this as *identical orbital representation* (IOR). The most

important virtue of this representation is that the exponential of a one-body operator \hat{A} transform a single-permanent wave function j_i into another single-permanent wave function $j_{i'}$ [26]

$$e^{\hat{A}} j_i = j_{i'}. \quad (12)$$

In particular, $\hat{B}(\mathbf{x})$ in Eq. (12) transforms a single permanent j_i into another single permanent $j_{i'}$. (In Appendix A we include a brief summary of properties of wave functions in IOR.)

E. Metropolis AFQMC

Standard AFQMC calculations [14] employ Metropolis Monte Carlo to compute various ground-state observables,

$$\begin{aligned} \hat{A}_{gs} &= \frac{\int d\mathbf{x}_m d\mathbf{y}_n \mathcal{P}_{gs} \hat{A} \mathcal{P}_{gs}}{\int d\mathbf{x}_m d\mathbf{y}_n \mathcal{P}_{gs}} \\ &= \frac{\int d\mathbf{x}_m d\mathbf{y}_n \mathcal{P}_{gs} \hat{A} \mathcal{P}_{gs}}{\int d\mathbf{x}_m d\mathbf{y}_n \mathcal{P}_{gs}} \\ &= \frac{\int d\mathbf{x}_m d\mathbf{y}_n \mathcal{P}_{gs} \hat{A} \mathcal{P}_{gs}}{\int d\mathbf{x}_m d\mathbf{y}_n \mathcal{P}_{gs}}; \end{aligned} \quad (13)$$

where

$$\begin{aligned} \mathcal{D}(\mathbf{x}_m; \mathbf{y}_n) &= \int d\mathbf{x}_m \int d\mathbf{y}_n \mathcal{P}(\mathbf{x}_m) \mathcal{P}(\mathbf{y}_n); \\ \mathcal{P}(\mathbf{x}_m; \mathbf{y}_n) &= \int d\mathbf{x}_m \int d\mathbf{y}_n \mathcal{P}(\mathbf{x}_m) \mathcal{P}(\mathbf{y}_n); \end{aligned}$$

and in the last line we have introduced the shorthand

$$\begin{aligned} \mathcal{H}(\mathbf{x}_m) &= \int d\mathbf{x}_m \mathcal{P}(\mathbf{x}_m); \\ \mathcal{J}(\mathbf{y}_m) &= \int d\mathbf{y}_m \mathcal{P}(\mathbf{y}_m); \end{aligned}$$

The Metropolis simulation is carried out by sampling the probability density function defined by the integrand in the denominator. Given the choice of \mathcal{P} in the identical-orbital representation, this readily applies to bosons, which is how the model calculation by Sugiyama and Koonin [14] was done. The total length of the imaginary time is predetermined by and the number of \hat{B} operators in the product.

III. NEW METHOD FOR BOSONS

In this paper we formulate a new approach for ground-state calculations of bosons with branching random walks. There

are several advantages in implementing the Monte Carlo sampling as a random walk process. It is a true ground-state formalism with open-ended random walks which allow projection to long enough imaginary-times. The sampling process can be made much more efficient than in standard AFQMC, by virtue of importance sampling with \mathcal{P} to guide the random walks. It also leads to a universal approach for bosons and fermions, where it is necessary to use the random walk formalism in order to implement a constraint to deal with the sign and complex-phase problems [19, 22].

A key observation is that we can choose an IOR single-permanent wave function as the initial wave function j_T . At each imaginary timestep n in the projection in Eq. (3), the wave function is stochastically sampled by a collection of single-permanent wave functions $f_j^{(i)}$, where the index i (in Cursive letter) is different from the basis index i . From Eqs. (9) and (12), we see that, with each walker $j_i^{(0)}$ initialized to j_T in IOR, the resulting projection will lead to a superposition of single-permanent wave functions, all of which are in IOR.

Each permanent evolves by the stochastic application of \mathcal{P}_{gs} , as follows: we randomly sample \mathbf{x} from the probability

density function $p(\mathbf{x})$, then apply $\hat{B}(\mathbf{x})$ on $j_i^{()}$:

$$j_i^{(+)} \hat{B}(\mathbf{x}) j_i^{()}; \quad (14)$$

We will call these permanents *random walkers*. The collection of these random walkers at each imaginary-time step is also referred to as *population*.

The population must first be equilibrated so that the ground-state distribution is reached. After equilibrium the ground state is given stochastically by the collection of single-permanent wave functions $f j_i^{()}$:

$$j_0^{()} = \sum_i^X j_i^{()}; \quad (15)$$

Measurement of ground-state observables can then be carried out.

The random walk process naturally causes the walker's orbitals to fluctuate. In order to increase sampling efficiency, we may associate a *weight* factor w_i to each walker $j_i^{()}$. For example, we can use the walker's amplitude as the weight factor:

$$w_i = \frac{p}{h_{ij_i^{()}}};$$

A better definition of the weight will be introduced later when we discuss importance sampling. We duplicate a walker when its weight exceeds a preset threshold. Conversely, walkers with small weight (lower than a predetermined limit) should be removed with the corresponding probability. In this way, the walkers will have roughly the same weight. This results in a branching random walk.

A. Measurement: “brute force” and mixed estimators

The ground-state value of an observable \hat{A} is its expectation value with the ground-state wave function:

$$\langle \hat{A} \rangle_{\text{g.s.}} = \frac{\langle j_0^{()} | \hat{A} | j_0^{()} \rangle}{\langle j_0^{()} | j_0^{()} \rangle}; \quad (16)$$

In principle, we can use the same Monte Carlo samples as both $j_0^{()}$ and $j_i^{()}$. A “brute force” measurement on population $f j_i^{()}$ at imaginary-time is then given by

$$\langle \hat{A} \rangle_{\text{bf}}^{()} = \frac{\sum_{ij} h_{ij}^{()} \hat{A} j_i^{()}}{\sum_{ij} h_{ij}^{()} j_i^{()}}; \quad (17)$$

and the estimator $\langle \hat{A} \rangle_{\text{bf}}$ is the average of such measurements. The “brute force” estimator is not useful in real-space based QMC methods such as diffusion Monte Carlo, because the overlaps between different walkers would lead to δ -functions. Here the walkers are non-orthogonal mean-field wave functions, and Eq. (17) is well defined in principle. The estimator is exact for all observables in the limit of large N_{wLKr} . The ground-state energy estimated in this way is variational, namely, the computed energy lies higher than the exact value

(outside of the statistical errorbar) and converges to the exact value as N_{wLKr} is increased. In practice, however, the usefulness of the “brute force” estimator is limited to smaller systems. In general it will have large variances. Reducing the variance is expensive because $\langle \hat{A} \rangle_{\text{bf}}$ scales as $O(N_{\text{wLKr}}^2)$, where N_{wLKr} is the size of the population used to represent $j_0^{()}$.

The simplest approach to measuring the observables is the mixed estimator, i.e.

$$\langle \hat{A} \rangle_{\text{mix}} = \frac{\langle j_0^{()} | \hat{A} | j_0^{()} \rangle}{\langle j_0^{()} | j_0^{()} \rangle}; \quad (18)$$

For example, to compute the ground-state energy, we can introduce the so-called local energy $E_L[j_T;]$:

$$E_L[j_T;] = \frac{\langle j_T^{()} | \hat{H} | j_T^{()} \rangle}{\langle j_T^{()} | j_T^{()} \rangle}; \quad (19)$$

The ground state energy is obtained from the weighted sum of the local energies associated with each walker:

$$E_{\text{mix}} = \frac{\sum_i h_{ij_T^{()}} E_L[j_T;]}{\sum_i h_{ij_T^{()}}}; \quad (20)$$

The local energy for each walker can be computed using the formula given in Appendix A.

The mixed estimator in Eq. (18) is exact only if the operator \hat{A} commutes with the Hamiltonian. Otherwise, a systematic error arises. Nonetheless the mixed estimator often gives an improvement over the purely variational estimator:

$$\langle \hat{A} \rangle_{\text{mix}} = \frac{\langle j_T^{()} | \hat{A} | j_T^{()} \rangle}{\langle j_T^{()} | j_T^{()} \rangle}; \quad (21)$$

Two formulas are often employed to correct for the systematic error:

$$\langle \hat{A} \rangle_{\text{extrap1}} = 2\langle \hat{A} \rangle_{\text{mix}} - \langle \hat{A} \rangle_{\text{T}}; \quad (22)$$

$$\langle \hat{A} \rangle_{\text{extrap2}} = \frac{\langle \hat{A}^2 \rangle_{\text{mix}}}{\langle \hat{A} \rangle_{\text{T}}}; \quad (23)$$

The second formula is useful for quantities such as density profile, where it must be nonnegative everywhere. These corrections are good only if $j_T^{()}$ does not differ significantly from $j_0^{()}$. In general, we need the back-propagation scheme to recover the correct ground-state properties. We will describe this method after introducing importance sampling.

B. Importance sampling

In practice, the efficiency of the bare random walk described earlier is very low, because the random walks “randomly” sample the Hilbert space, and the weights of the walkers fluctuate greatly. This results in large statistical noise. We formulate an importance sampling procedure [19, 22]—using the information provided by the trial wave function $j_T^{()}$ —to guide the random walk into the region where the expected contribution to the wave function is large.

1. Importance-sampled random walkers

An importance-sampled walker also consists of a permanent and a weight, although the weight will be redefined according to the projected overlap of the permanent with the trial wave function. The purpose is to define a random walk process which will lead to a stochastic representation of the ground-state wave function in the form

$$j_0 = \sum_i w_i \frac{j_i}{h_T j_i}; \quad (24)$$

where w_i is the new weight of the walker. The overlap enters to redefine the weight factor such that walkers which have large overlap with j_T will be considered “important” and will tend to be sampled more. Such walkers will also have greater contributions in the measured observables. Since the permanent now appears as a ratio $j_i/h_T j_i$, its normalization is no longer relevant and can be discarded, unlike in the unguided random walk. The only meaningful information in j_i is its position in the permanent space.

2. Modified auxiliary-field transformation

Now we describe the random walk process for the modified walkers. The goal is to modify P_{gs} in Eq. (9) such that the random walk process leads to random walkers with the characteristics described above in Eq. (24). The basic idea is the same as that in Ref. 19. The main difference is that here we are dealing with bosons. In addition the HS fields in Ref. 19 are discrete Ising-like, which allowed simplifications in the importance sampling, while here the auxiliary fields are continuous and thus a more general formalism will be developed. Our mathematical derivation here follows that of Ref. 22. Up to now we have assumed that $h_T j_i$ is real and positive. There is therefore no additional subtlety with the meaning of importance sampling and the correct form of the overlap to use, which Ref. 22 addressed in the context of fermionic calculations with general interactions.

To derive the importance-sampled propagator, we plug Eq. (24) into Eq. (3b). We will focus on the two-body propagator, which is evaluated stochastically and is therefore affected by importance sampling in a non-trivial way.

The modified propagator, \mathbb{P}_{gs} , consists of two parts. The first part is the transformation introduced in Eq. (5), which we now rewrite in the following form:

$$e^{\frac{1}{2} \phi^2} = \frac{1}{2} \int_{-1}^1 dx e^{\frac{1}{2} x^2} e^{\mathbf{x} \cdot \mathbf{x}} e^{\frac{1}{2} \mathbf{x}^2} e^{\mathbf{x} \cdot \mathbf{x}}; \quad (25)$$

where we have added an arbitrary shift \mathbf{x} to the auxiliary field \mathbf{x} in the auxiliary-field operator. This is a change of variable in the integral on the right-hand side and does not alter the result of the integral. The new propagator \mathbb{P}_{gs} must preserve the representation of j_0 in the form of Eq. (24); this dictates

that the walkers propagate in the following manner:

$$w_i^{(+)} = \frac{j_i^{(+)} i}{h_T j_i^{(+)} i} \quad w_i^{(-)} = \frac{j_i^{(-)} i}{h_T j_i^{(-)} i}; \quad (26)$$

From this requirement comes the second part of the modified propagator, which is the overlap ratio $h_T j_i^{(+)} i = h_T j_i^{(-)} i$. This factor is obtained by bringing the term $h_T j_i^{(+)} i$ in Eq. (26) to the right-hand side. It depends on j_T and the specific path in auxiliary-field space, and will “guide” the random-walk toward the region where $h_T j_i$ is large.

Combining the two parts gives an importance-sampled propagator of the form

$$\mathbb{P}_{gs}[\] = \int d\mathbf{x} p(\mathbf{x}) W(\mathbf{x};) \hat{B}(\mathbf{x} \cdot \mathbf{x}); \quad (27)$$

where

$$W(\mathbf{x};) = \frac{h_T \hat{B}(\mathbf{x} \cdot \mathbf{x}) j_i}{h_T j_i} e^{\mathbf{x} \cdot \mathbf{x}} e^{\frac{1}{2} \mathbf{x} \cdot \mathbf{x}} \quad (28)$$

is the aggregate of all the scalar prefactors in the modified propagator. This propagator takes $f w_i^{(-)}; j_i^{(-)} i$ and advances the population to $f w_i^{(+)}; j_i^{(+)} i$, both of which represent j_0 in the form of Eq. (24).

Monte Carlo sampling of the new propagator \mathbb{P}_{gs} is similar to the one without importance sampling. We sample \mathbf{x} from a normal Gaussian distribution, and apply the operator $\hat{B}(\mathbf{x} \cdot \mathbf{x})$ to the current walker $j_i^{(-)} i$. But now we accumulate an extra multiplicative weight factor $W(\mathbf{x}; i^{(-)})$ every time we apply Eq. (27):

$$j_i^{(+)} i = \hat{B}(\mathbf{x} \cdot \mathbf{x}) j_i^{(-)} i \quad (29a)$$

$$w_i^{(+)} = W(\mathbf{x}; i^{(-)}) w_i^{(-)}; \quad (29b)$$

Here we use the customary notation of vector dot product, e.g. $\mathbf{x} \cdot \mathbf{x} = \sum_i x_i x_i$. Note that the weight factor $W(\mathbf{x}; i^{(-)})$ depends on both the current $i^{(-)}$ and future $i^{(+)}$ walker positions.

3. The optimal choice for auxiliary-field shift \mathbf{x}

The optimal importance sampling is achieved when each random walker contributes equally to the estimator. We therefore choose \mathbf{x} to minimize the fluctuation in the weight factor w_i . The fluctuation in w_i will be minimized if we minimize the fluctuation in the prefactor Eq. (28). We do so by requiring the partial derivatives of this prefactor to vanish with respect to x_i at its average ($x_i = 0$):

$$\frac{\partial}{\partial x_i} \frac{h_T \hat{B}(\mathbf{x} \cdot \mathbf{x}) j_i}{h_T j_i} e^{\mathbf{x} \cdot \mathbf{x}} e^{\frac{1}{2} \mathbf{x} \cdot \mathbf{x}} \Big|_{x_i=0} = 0;$$

It is sufficient to expand the exponentials in terms of \mathbf{x}_i and require the term linear in \mathbf{x}_i to vanish, since this is the leading term, containing \mathbf{p} . The others contain higher-order terms and are vanishingly small as $\mathbf{p} \rightarrow 0$. The best choice for \mathbf{x}_i that satisfies this requirement is

$$\mathbf{x}_i = \frac{\mathbf{p} \cdot \mathbf{h}_T \mathbf{j}_i \mathbf{j}_i}{h_T \mathbf{j}_i \mathbf{j}_i} \mathbf{p} \cdot \mathbf{v}_i : \quad (30)$$

This choice depends on the current walker position as well as $\mathbf{j}_T \mathbf{i}$, which is to be expected, since the objective for the shift is to guide the random walk toward the region where $h_T \mathbf{j}_i \mathbf{j}_i$ is large. With \mathbf{x} determined, the algorithm for the random walk, as given in Eq. (29), is now completely specified.

4. Local energy approximation

We can furthermore approximate the prefactor $W(\mathbf{x}; \mathbf{j})$ in Eq. (28) to obtain a more elegant and compact expression. After rewriting the prefactor in the form of an exponential, expanding $\hat{E}(\mathbf{x}, \mathbf{x})$ in terms of \mathbf{x} , and ignoring terms higher than $O(\mathbf{x}^2)$ in the exponent, we obtain

$$Y_i = e^{\frac{1}{2} (\mathbf{x} \cdot \mathbf{v}_i^2) (\mathbf{v}_i^2 \cdot \mathbf{v}_i^2)} e^{\frac{1}{2} \mathbf{v}_i^2}; \quad (31)$$

where

$$\mathbf{v}_i^2 = \frac{h_T \mathbf{j}_i^2 \mathbf{j}_i \mathbf{i}}{h_T \mathbf{j}_i \mathbf{j}_i}; \quad (32)$$

The product is over the basis index i , which should be distinguished from the walker index i . The latter is held fixed here. The first exponential in Eq. (31) can be ignored by noting that the average value of \mathbf{x}_i^2 with respect to the Gaussian probability density function is unity. Setting $\mathbf{x}_i^2 \rightarrow 1$, i.e., evaluating the exponential at the mean value $h \mathbf{x}_i^2 \mathbf{i}$, is justified because \mathbf{v}_i^2 and \mathbf{v}_i^2 do not change drastically within one timestep. We also note that $\mathbf{v}_i^2 = h_T \mathbf{j}_i^2 \mathbf{j}_i \mathbf{i} = h_T \mathbf{j}_i \mathbf{j}_i$, which is the mixed-estimator of the potential energy with respect to the walker $\mathbf{j}_i \mathbf{i}$. Combining this term with the similar contribution from the kinetic propagator, we obtain a simple, approximate expression for Eq. (28):

$$W(\mathbf{x}; \mathbf{j}_i) = e^{(E_T + E_L[\mathbf{T}; \mathbf{j}_i])}; \quad (33)$$

where $E_L[\mathbf{T}; \mathbf{j}_i]$ is the local energy of \mathbf{j}_i as defined in Eq. (19). Note that, contrary to Eq. (28), this form depends only on the current walker position and not the future, although in practice a symmetrized version can be used which replaces the local energy by the average of the two. For a good trial wave function, the local energy fluctuates less in the random walk. If the trial wave function is the exact ground-state wave function, the local energy becomes a constant and the weight fluctuation is altogether eliminated. This bears a close formal resemblance to the importance-sampled diffusion Monte Carlo method.

The algorithm resulting from Eq. (33) is an *alternative* to Eq. (28). The two are identical and exact in the limit $\mathbf{p} \rightarrow 0$, but can have different Trotter errors.

C. Measurement: back propagation

With importance sampling, the mixed estimator in Eq. (18) is given by:

$$h \hat{A}_{m, ix} = \frac{\sum_i W_i \frac{h_T \hat{A} \mathbf{j}_i \mathbf{i}}{h_T \mathbf{j}_i \mathbf{j}_i}}{\sum_i W_i}; \quad (34)$$

For example, the ground-state energy is

$$E_{m, ix} = \frac{\sum_i W_i E_L[\mathbf{T}; \mathbf{j}_i]}{\sum_i W_i}.$$

As mentioned earlier, the normalization of \mathbf{j}_i is irrelevant because \mathbf{j}_i only appears in ratios in any formula that defines the algorithm: Eqs. (24), (28), (30), (33), and Eq. (34). We can (and should) normalize the permanent as needed, and discard the resulting normalization factor.

The mixed estimator is often inadequate for computing observables whose operators do not commute with the Hamiltonian. In some cases the error due to this noncommutation is unacceptable. For example, the condensate fraction in the attractive trapped Bose-Hubbard model is greater than 100% if the Green's function $h \mathbf{x}_{C_j}^Y \mathbf{i}$ is estimated using the mixed estimator. Therefore we have to propagate the wave functions on both the right- and the left-hand side of the operator:

$$h \hat{A}_{b_p} = \frac{h_T \mathbf{j}_p \mathbf{b}_p \hat{A} \mathbf{j}_0 \mathbf{i}}{h_T \mathbf{j}_p \mathbf{b}_p \mathbf{j}_0 \mathbf{i}}; \quad (35)$$

This estimator approaches the exact expectation value in Eq. (16) as \mathbf{b}_p is increased. Zhang and co-workers proposed a back-propagation technique [19] that reuses the auxiliary-field “paths” from different segments of the simulation to obtain $h \mathbf{b}_p \mathbf{j}_0 \mathbf{i} = h_T \mathbf{j}_p \mathbf{b}_p \mathbf{j}_0 \mathbf{i}$, while avoiding the $N_{w, kr}^2$ scaling of a brute-force evaluation with two separate populations for $h \mathbf{j}_0 \mathbf{i}$ and $\mathbf{j}_0 \mathbf{i}$. Here we give a more formal derivation and description of the technique, and implement it to bosons.

At imaginary-time τ , the population is $\mathbf{f} \mathbf{j}_i^{(\tau)} \mathbf{i}$, which represents $\mathbf{j}_0 \mathbf{i}$ in the form of Eq. (24). The propagator in the denominator can be viewed equivalently as operating on the left or the right. The latter view is precisely the “normal” importance-sampled random walk from $\tau=0$ to the future time $\tau + \mathbf{b}_p$, which consists of $n_{b_p} = \mathbf{b}_p / \Delta \tau$ steps. We first assume that there is no branching (birth/death of walkers), i.e., the weights are fully multiplied according to Eq. (28). The random walk of each walker will generate a path in auxiliary-field space. For convenience we will denote the path-dependent operator $\hat{E}[\mathbf{x}_i^{(\tau)}; \mathbf{j}_i^{(\tau)}]$ by $\hat{E}_i^{(\tau)}$, and weight factor $W(\mathbf{x}_i^{(\tau)}; \mathbf{j}_i^{(\tau)})$ by $W_i^{(\tau)}$. Further we will denote the time-ordered product of $\hat{E}_i^{(\tau)}$ from imaginary-time $\tau=0$ by $\hat{E}_i^{(0; \tau)}$, and correspondingly the product of $W_i^{(\tau)}$ by $W_i^{(0; \tau)}$. Each path defines a product

$$\frac{1}{h_T \mathbf{j}_i^{(0)} \mathbf{i}} W_i^{(0; \tau)} \hat{E}_i^{(0; \tau)} h_T \mathbf{j}_i^{(\tau)} \mathbf{i}; \quad (36)$$

Collectively these products give a stochastic representation of $e^{-\beta_p H}$.

Replacing the operator $e^{-\beta_p H}$ in the numerator and denominator of Eq. (35) with Eq. (36), and using the expression for j_0 given by Eq. (24), we obtain

$$\hat{h}^i_{bp} = \frac{\prod_{i=0}^P h_{i,T} \prod_{h=1}^{j_{i,T}} \frac{1}{j_{i,T}} W_i^{(0)} \hat{B}_i^{(0)} \hat{A} w_i^{(j_i)} j_i^{(j_i)} i}{\prod_{i=0}^P h_{i,T} \prod_{h=1}^{j_{i,T}} \frac{1}{j_{i,T}} W_i^{(0)} \hat{B}_i^{(0)} w_i^{(j_i)} j_i^{(j_i)} i} : \quad (37)$$

Using the propagation relation in Eq. (29), we can show that

$$\hat{B}_i^{(0)} w_i^{(0)} w_i^{(j_i)} j_i^{(j_i)} i = w_i^{(0)} j_i^{(0)} i; \quad (38)$$

i.e., the denominator in Eq. (37) reduces to $\prod_{i=0}^P w_i^{(0)}$. This result is to be expected, and can also be seen by completing the n_{bp} steps of the “normal” random walk we discussed above. With importance sampling, the Monte Carlo estimate of the denominator is simply given by the weights at time 0.

To simplify the numerator we associate a *back-propagated* wave function with each walker $j_i^{(j_i)} i$

$$j_i^{(bp)} i \quad h_{i,T} \hat{B}_i^{(+\beta_p)} j_i^{(j_i)} i : \quad (39)$$

Note that each of these $j_i^{(j_i)} i$ originates from the trial wave function $j_T i$, and is propagated by applying the \hat{B} 's in *reverse* order, as implied by the Hermitian conjugation. We may then write Eq. (37) in the following form:

$$\hat{h}^i_{bp} = \frac{\prod_{i=0}^P w_i^{(0)} h_{i,T} \hat{B}_i^{(+\beta_p)} j_i^{(j_i)} i}{\prod_{i=0}^P w_i^{(0)} j_i^{(j_i)} i} : \quad (40)$$

The estimators in Eqs. (35) and (40) parallel that of the standard AFQMC estimator in Eq. (13). The j_i 's and h_j 's have similar meanings. The only difference lies in how the paths are generated. Here an open-ended random walk is used to advance an ensemble of paths from 0 to 0 , which result in fluctuating weights that represent the path distribution. In standard AFQMC a fixed length path (corresponding to $\beta_p + \epsilon_{eq}$, with ϵ_{eq} being the minimum time for equilibration or, failing that, the maximum time that can be managed by the calculation) is moved about by the Metropolis algorithm, which eliminates branching by the acceptance/rejection step. In other words, the estimators in Eq. (13) and Eq. (40) are the same except for the weights.

Eq. (40) defines an algorithm for obtaining the estimate of \hat{h}^i_{bp} via the following steps:

1. A population is recorded as $f j_i^{(j_i)} i$;
2. as the random walk continues, the path history is kept for a time interval β_p ;

3. the population $f j_i^{(bp)} i$ is then generated by back-propagation using Eq. (39);
4. this population is matched in a one-to-one manner to $f j_i^{(j_i)} i$, weighted by the weight *at the later time*, $w_i^{(j_i)}$, and the estimator is formed.

In the back-propagation the propagators are, as shown in Eq. (39), identical to those in the forward direction, but in reverse order in imaginary-time. As in the normal walk, the normalization of $j_i^{(bp)} i$ does not enter in the estimator. Similar to the mixed estimator, this procedure can be repeated periodically to improve statistics. Evidently this estimator is exact in the limit of large β_p .

We have assumed that there is no branching within the interval β_p . In practice, a population control scheme is often used which causes birth/death of walkers. This does not affect the derivation above or the basic algorithm. The effect on the implementation is that a list of ancestry links must be kept for the forward steps, which indicates the parent of each walker at each step in the imaginary-time duration β_p . As a result of branching, two or more h_j 's may share the same segment of the paths in their “past” and the same parent $j_i^{(j_i)} i$. The estimator remains exact for large β_p . Branching or weight fluctuation does have a more serious practical implication, however. As β_p is increased, more and more h_j 's will be traced back to the same parent $j_i^{(j_i)} i$. Or equivalently, fewer and fewer permanents in the set $f j_i^{(j_i)} i$ will contribute to the estimator. This results in a loss of efficiency or an increase in variance. Better importance sampling will help improve the situation, often greatly, by reducing fluctuations in weights, although the problem will always occur at large enough β_p . In our applications to date we have rarely encountered the problem and find that the computed observables converge quite rapidly (see section V for illustrative results).

IV. TRAPPED BOSON GAS: MODEL AND IMPLEMENTATIONS OF QMC AND GP METHODS

In this section we discuss the model we use to describe a single-species, Bose atomic gas with pair-wise contact interaction, confined in a harmonic trap in one- or three-dimensions. We then describe the implementations of both our QMC method and the standard mean-field GP approach to study this model. Numerical results will be presented in the following section, Sec. V.

A. Model

We use an effective potential characterized by the low energy atom-atom scattering length, a_s . The two-body interaction takes a simple form

$$U(r_1, r_2) = \frac{4 a_s^2}{m} \delta(r_1 - r_2) : \quad (41)$$

For this effective potential to be valid, several assumptions are made; for example, the dominant effect is from s -wave scattering, and \bar{a}_s is much smaller than the average inter-particle spacing. For more details we refer the reader to Ref. 3. In the alkali gases these conditions are in general well met, and the model potential can be expected to give qualitative informa-

tion, although care must be taken to validate the conditions.

We now derive the Bose-Hubbard model from the standard many-body Hamiltonian of the trapped boson problem in d -dimension. In the continuous, real space, the Hamiltonian is given by:

$$\hat{H} = \hat{K} + \hat{V} = \int d^3r \hat{\psi}^\dagger(r) \left(-\frac{\hbar^2}{2m} \nabla^2 + \frac{1}{2} m \omega_0^2 r^2 \right) \hat{\psi}(r) + \frac{1}{2} \int d^3r_1 d^3r_2 \hat{\psi}^\dagger(r_1) \hat{\psi}^\dagger(r_2) \hat{V}(r_1, r_2) \hat{\psi}(r_2) \hat{\psi}(r_1) ; \quad (42)$$

The first term is the one-body Hamiltonian \hat{K} , which consists of the kinetic energy and the (external) confinement potential. \hat{V} is the interaction Hamiltonian, which is the sum of all the two-body potentials. The characteristic trap frequency is ω_0 , which is related to the so-called oscillator length scale by $a_{ho} = \sqrt{\hbar / m \omega_0}$.

We introduce a real-space lattice, with a linear dimension of

L , in a simulation cell of volume $(2x_b)^d$. The lattice spacing is therefore $\& = 2x_b/L$. Further we will consider only a spherically symmetric trap here for simplicity. We truncate the simulation cell accordingly and assume that the wave function is negligible outside the maximum sphere enclosed by the cell. (Generalization to inhomogeneous traps is straightforward.)

The discretized Hamiltonian corresponding to Eq. (42) is

$$\hat{H} = \sum_i \left(-\frac{\hbar^2}{2m} \nabla_i^2 + \frac{1}{2} m \omega_0^2 \mathbf{r}_i^2 \right) c_i^\dagger c_i + \frac{1}{2} \sum_{i,j} \bar{a}_s^d \hat{\psi}_i^\dagger \hat{\psi}_i^\dagger \hat{\psi}_j \hat{\psi}_j ; \quad (43)$$

where c_i^\dagger and c_i are the usual creation and annihilation operators at site i . The Hubbard parameters t , U , and \bar{a}_s^d are related to the real, physical parameters as follows:

$$t = \frac{1}{2\&} \quad (44a)$$

$$U = \frac{4 \bar{a}_s}{\&^d} \quad (44b)$$

$$= \frac{\&^2}{a_{ho}^4} ; \quad (44c)$$

where for simplicity we have set $\hbar = m = 1$. The lattice coordinate \mathbf{x}_i is related to the real coordinate by $\mathbf{x}_i = (L/2x_b)\mathbf{r}_i$, and \mathbf{r}_0 is the lattice coordinate of the trap's center. Note that a_s is the true scattering length only in three-dimensional systems. Nonetheless we will retain the symbol a_s in Eq. (44b) as a convenient measure of the interaction strength in any dimension.

In the discretized model our resolution is limited by the lattice spacing. This is consistent with the conditions of validity of the model interaction in Eq. (41), as it in a sense “integrates out” the short-range dynamics. In this model our lattice constant must be much smaller compared to the average in-

terparticle spacing, but larger than the scattering length:

$$\bar{a}_s \ll \& \ll 1/d ; \quad (45)$$

With negative a_s , the particles tend to “lump” together due to the gain in the interaction energy. This is a situation where we especially have to be aware of the validity of the effective potential. As mentioned we will do a consistency check at the end of the calculation to ensure that the occupancy of the lattice points are less than unity.

B. Implementation of QMC

Implementation of our QMC method for this model is straightforward. The number of basis M is equal to the number of lattice sites inside the truncated sphere of radius x_b . The two-body term in Eq. (43) is in the desired form of Eq. (6). With a negative U , the HS transformation in Eq. (7) leads to M auxiliary fields, with one-body propagators in the form of $\exp(-\int \mathbf{x}_i \hat{n}_i)$, where $\hat{n}_i = c_i^\dagger c_i$ is the density operator. Our trial wave function $\prod_i \psi_i$ is the Gross-Pitaevskii (GP) wave function ψ_{GP} , which we describe in the next subsection.

We mention here a technical point in the implementation. The ground-state projection in our method involves the appli-

cation of one-body propagator in the form of $e^{\hat{K}}$ on a single-permanent wave function ψ . This usually translates into a matrix-vector multiplication in the computer program, which generally costs $O(M^2)$. Often there are special properties of \hat{A} that can be exploited to evaluate the one-body propagator more efficiently. In the Bose-Hubbard Hamiltonian, the only non-diagonal part of the Hamiltonian in real space is the kinetic operator in \hat{K} . We can separate it from the other one-body operators and apply the kinetic propagator in momentum space. Wave functions are quickly translated between these two representations using the Fast Fourier transform (FFT). In this way, the actual application of $e^{\frac{1}{2}\hat{K}}$ involves only diagonal matrices; thus the overall cost for each $e^{\frac{1}{2}\hat{K}}$ operation is reduced to $O(M \log M)$. We observe in our calculations that the additional Trotter error is much smaller than the error already introduced in the original breakup, Eq. (4).

C. Implementation of Gross-Pitaevskii self-consistent equation

The Gross-Pitaevskii (GP) wave function ψ_{GP} is the single-permanent wave function

$$\psi_{GP}(\mathbf{r}_1; \mathbf{r}_2; \dots; \mathbf{r}_N) = \psi(\mathbf{r}_1) \psi(\mathbf{r}_2) \dots \psi(\mathbf{r}_N) \quad (46)$$

which minimizes the expectation value of the ground-state energy. Such a wave function satisfies the self-consistent Gross-Pitaevskii equation [27, 28, 29]

$$\begin{aligned} & \frac{\hbar^2}{2m} \nabla^2 \psi(\mathbf{r}) + \frac{1}{2} m \omega_0^2 \mathbf{r}^2 \psi(\mathbf{r}) - \epsilon_0 \psi(\mathbf{r}) \\ & + \frac{N}{N-1} \frac{14}{m} a_s \hbar^2 \nabla^2 \psi(\mathbf{r}) \psi(\mathbf{r}) = \epsilon \psi(\mathbf{r}) : \end{aligned} \quad (47)$$

[We keep the prefactor $(N-1)/N$, since we will study both large and small values of N .]

To compare our QMC results to those of mean-field, we carry out GP calculations on the same lattice systems. The discretized GP Hamiltonian in the second-quantized form is:

$$\begin{aligned} \hat{H}_{GP} = & \sum_{\mathbf{i}, \mathbf{j}} \sum_{n,n(i)} \psi_{\mathbf{i}}^\dagger \psi_{\mathbf{j}} - 2d \sum_{\mathbf{i}} \psi_{\mathbf{i}}^\dagger \psi_{\mathbf{i}} \\ & + \frac{1}{2} \sum_{\mathbf{i}} \psi_{\mathbf{i}}^\dagger \psi_{\mathbf{i}}^2 \epsilon_0 \psi_{\mathbf{i}}^\dagger \psi_{\mathbf{i}} \\ & + \frac{N}{N-1} \frac{1}{U} \sum_{\mathbf{i}} n_{\mathbf{i}} \psi_{\mathbf{i}}^\dagger \psi_{\mathbf{i}} - \frac{1}{2} n_{\mathbf{i}}^2 : \end{aligned} \quad (48)$$

Here $n_{\mathbf{i}}$ is the expectation value of the density operator:

$$n_{\mathbf{i}} = \frac{\langle \psi_{GP} | \psi_{\mathbf{i}}^\dagger \psi_{\mathbf{i}} | \psi_{GP} \rangle}{\langle \psi_{GP} | \psi_{GP} \rangle} : \quad (49)$$

We have implemented two methods for solving the GP equation. The *first* is the usual self-consistent iterative approach. We generate an initial density profile, $n_{\mathbf{i}}^{(0)}$, by solving the non-interacting Hamiltonian (with $U = 0$). The density is fed back to construct the initial Hamiltonian $\hat{H}_{GP}^{(0)}$ in (48). Direct diagonalization of this one-body Hamiltonian yields its

ground state $|\psi_{GP}^{(1)}\rangle$. We thus obtain an updated density $n_{\mathbf{i}}^{(1)}$ and a better Hamiltonian $\hat{H}_{GP}^{(1)}$. This procedure is iterated until the desired convergence criterion is satisfied. We choose our convergence condition to be:

$$\frac{\int d\mathbf{r} |\psi^{(t+1)}(\mathbf{r}) - \psi^{(t)}(\mathbf{r})|^2}{\int d\mathbf{r} |\psi^{(t+1)}(\mathbf{r}) + \psi^{(t)}(\mathbf{r})|^2} < \epsilon ; \quad (50)$$

where ϵ is a small number (usually on the order of 10^{-13} for double precision numbers).

The *second* method we use to solve Eq. (48) avoids the diagonalization procedure. It is closely related to the QMC method, both computationally and formally (see Sec. VI). We use the ground-state projector $e^{-\hat{H}_{GP}}$:

$$|\psi_{GP}\rangle = \frac{e^{-\hat{H}_{GP}} |\psi^{(0)}\rangle}{\langle \psi^{(0)} | e^{-\hat{H}_{GP}} | \psi^{(0)} \rangle} : \quad (51)$$

The initial wave function is arbitrary and can be, for example, chosen again as the solution with $U = 0$. The feedback mechanism through the density profile $n_{\mathbf{i}}$ remains the same. By using the same Fast Fourier transform for the kinetic propagator as described in subsection IV B, a speed gain is obtained, especially for large systems. In practice we have often found this method to be a simpler and faster alternative to the first method of diagonalization and iteration. Note that the scalar term $\frac{1}{2} \frac{N-1}{N} U \sum_{\mathbf{i}} n_{\mathbf{i}}^2$ does not affect the projection process, but with it \hat{H}_{GP} corresponds to the original many-body Hamiltonian in that $\langle \psi_{GP} | \hat{H}_{GP} | \psi_{GP} \rangle = \langle \psi_{GP} | \hat{H} | \psi_{GP} \rangle$.

V. RESULTS

In this section we present results from our QMC and GP calculations in one-, two-, and three-dimensions. To validate our new QMC method and illustrate its behavior, the majority of the calculations will be on systems where exact results are available for benchmark. These include small lattices, which can be diagonalized exactly, and the case of attractive δ -function interactions in one dimension, where analytic solutions exist. For the purpose of presenting the method to facilitate implementation, some numerical results and comparisons are shown in detail to illustrate the behavior and characteristics of the method.

Most of the results we present here will be for attractive interactions, where the method is exact and is free of any phase problem [22] from complex propagators (see subsection V C). Such systems therefore provide a clean testground for our new method. In addition, with attractive interactions the condensate in 3-D is believed to collapse beyond a critical interaction strength or number of particles. Mean-field calculations [30] estimate the collapse critical point to be about $N a_s a_{ho} = 0.575$. The exact behavior of the condensate near the critical point is, however, not completely clear, as many-body effects are expected to have an impact. At the end of this section we will also show some preliminary results for larger systems with both attractive and repulsive interactions in 3-D.

We measure the ground-state expectation values of the following quantities: the ground-state energy, kinetic energy $\langle \hat{H} \rangle$, external confining potential $\langle \hat{V}_{\text{trap}} \rangle$, interaction energy $\langle \hat{V}_{2B} \rangle$, density profile $\langle \hat{n}_i \rangle$, and the condensate fraction (often abbreviated “cond.frac.” in the tables and figures). The condensate fraction is defined as the largest eigenvalue of the diagonalized density matrix [3]. If we write the one-body Green’s function matrix hc_{ij}^y in terms of its eigenvalues f_n and eigenvectors $f^{(i)}_n$:

$$hc_{ij}^y = \sum_n f_n \sum_{\alpha} f^{(\alpha)}_i f^{(\alpha)}_j;$$

then the largest eigenvalue divided by the total number of particles gives the condensate fraction.

A. Comparison with exact diagonalization: $a_s < 0$

The many-body Hamiltonian (43) can be diagonalized exactly for small systems to benchmark our QMC calculation. We compare our QMC results with exact diagonalization for a one-dimensional lattice of 13 sites, and study its behavior for different values of the interaction strength a_s and number of particles N .

The first system we study has 5 bosons, with $t = 2.676$, $U = 1.538$, $\mu = 0.3503$. These values correspond to the physical parameters $a_{ho} = 8546 \text{ \AA}$ and $a_s = 5.292 \cdot 10^{-6} \text{ \AA}^{-1}$. (Recall that, by our definition, a_s in 1-D does not have the dimension of length, and is not the scattering length itself.) Table I shows the comparison of the quantities computed using three methods: QMC, GP, and exact diagonalization (ED). The statistical uncertainty of QMC results are presented in parentheses. We see that the agreement between QMC and ED is excellent. GP makes significant errors here because of the sizable interaction strength as well as the small number of particles.

TABLE I: Comparison of QMC calculation against exact diagonalization (ED) and Gross-Pitaveskii (GP). The system has 13 sites, 5 particles, $t = 2.676$, $U = 1.538$, $\mu = 0.3503$. In the QMC calculation we use $\tau = 0.01$, $\tau_{BP} = 4.0$, and the GP solution as the trial wave function.

Type	g.s.energy	$\langle \hat{H} \rangle$	$\langle \hat{V}_{\text{trap}} \rangle$	$\langle \hat{V}_{2B} \rangle$	cond.frac.
ED	1.009	4.278	0.8427	6.129	95.59%
QMC	1.008 (2)	4.279 (3)	0.8423 (5)	6.129 (2)	95.59%
GP	0.493	3.919	0.7504	5.162	100%

To illustrate the convergence in imaginary-timestep τ , we show in Fig. 1 the total energy and the average trap energy $\langle \hat{V}_{\text{trap}} \rangle$. The former can be obtained exactly from the mixed estimator while the latter requires back propagation. To show the Trotter error, we have deliberately done the calculations up to rather large τ values. We see that both quantities converge to the exact results as $\tau \rightarrow 0$.

To illustrate the convergence of observables in back-propagation length, we show in Fig. 2 the various observables

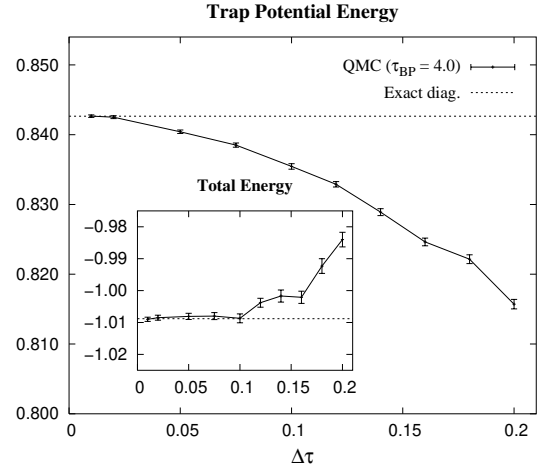


FIG. 1: Convergence of QMC observables with τ . The system has the same parameters as in Table I. Exact results are shown as dotted lines. Lines connecting QMC data are to aid the eye.

computed by QMC as a function of τ_{BP} . Separate calculations were done for different values of τ_{BP} . For all calculations, a small τ value of 0.01 was used. We see that all quantities converge to the exact results rather quickly, by $\tau_{BP} \approx 2$. (The total energy $\langle \hat{H} \rangle$ is of course exact for any τ_{BP} , including $\tau_{BP} = 0$.) As we see from the energy expectations, this is in fact a system with significant interaction effects. Alkali systems at the experimental parameters often have significantly weaker interaction strengths and the convergence rate is expected to be even faster.

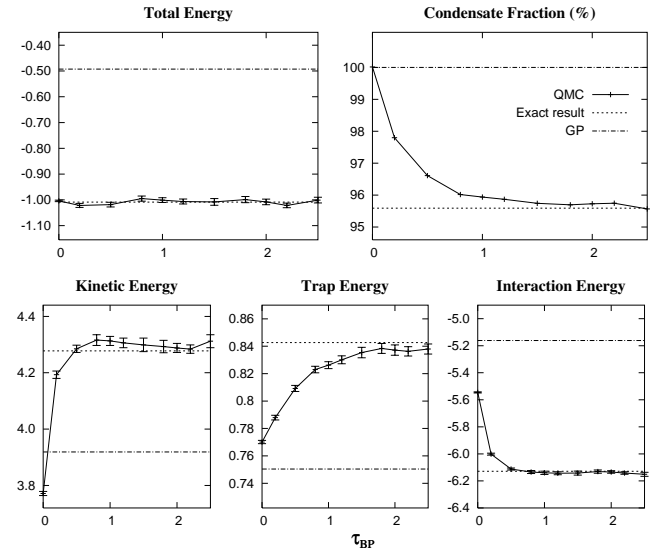


FIG. 2: Convergence of the computed observables versus τ_{BP} . The system is the same as in Table I. The different panels show five different observables. The horizontal axes are the back-propagation length. Exact results are shown as dotted lines, while GP results are dash-dotted lines. Solid lines are present only to aid the eye.

Our QMC method is exact and therefore independent of the trial wave function ψ_T , except for convergence rate and sta-

tistical errors. In Fig. 3 we show QMC results obtained using two different Ψ_T 's, the noninteracting solution and the GP wave function. The convergence of condensate fraction and trap energy are shown versus back-propagation time τ_{BP} for a system of 6 particles on 13 sites. The calculations lead to the same results. The quality of Ψ_T , however, does affect the variances of the observables and their convergence rates with τ_{BP} . For example, the noninteracting wave function, which disregards the two-body interaction, is more extended (in its density profile) than GP. Its mixed estimator is therefore worse than that with the GP trial wave function. The mixed-estimator for the ground-state energy is exact in both, but the variance is slightly larger with the former.

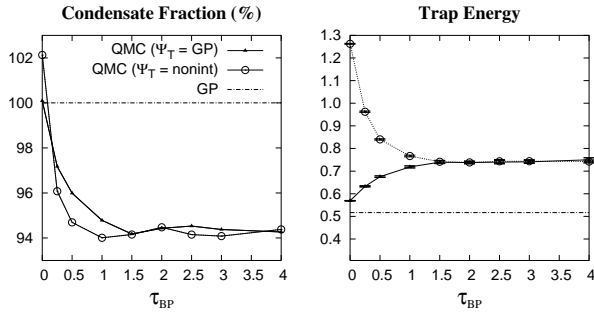


FIG. 3: Independence of QMC results on trial wave functions (“GP” for Gross-Pitaevskii, “nonint” for noninteracting solution). The system is the same as in Table I, except that here we use 6 particles. The horizontal axes are the back-propagation length. Lines connecting QMC data points are present only to aid the eye.

We now show results for different systems with N from 2 to 9 bosons, and varying interaction strengths. We note that if we keep the product $U/(N-1)$ constant, the Gross-Pitaevskii equation predicts the same *per-particle* energies and densities. For brevity, we shall refer to the curve in which $U/(N-1)$ is constant as the *GP isoline*. Deviation from the GP isoline is therefore an indication of the effect of many-body correlations. In order to show results on multiple systems at the same time we will scan GP isolines. Figure 4 shows the QMC and GP results as a function of the number of particles. In the GP calculations the per-particle quantities are constants. The QMC results, on the other hand, capture the effect of correlation. Both the total energy and the interaction energy are lowered from the GP results. The exact results deviate from GP more as the system becomes more correlated along the GP isoline, i.e. when U is increased or when N is decreased. Although N is too small here because of the limitation of ED, the results are representative of the general trend in larger systems (see below).

Figure 5 further illustrates the effect of particle correlation in this system. Although the exact interaction energy is lower than that of GP, the exact density profile is more extended. This is also manifested in the average trap potential energy $\langle \hat{V}_{\text{trap}} \rangle_{i=N}$, where the QMC results are $0.1981(8)$ and $0.1605(2)$ for $N = 2$ and 9 particles, respectively, while the GP value is 0.1501 . In GP, interaction energy is lowered by increasing particle overlap, namely by shrinking the profile.

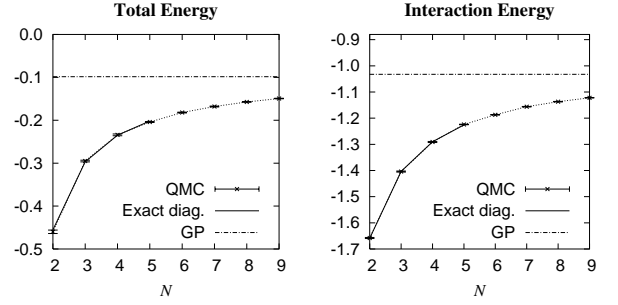


FIG. 4: Comparison of QMC, GP, and ED results for different systems. Calculations were done along a GP isoline $U/(N-1) = 2.30t$ for up to nine particles in 13 sites. The graphs show the total and interaction energies *per particle*. QMC and exact results are indistinguishable. GP is accurate in the limit of weak correlation but deviates more from the exact results as the system becomes more correlated. The solid lines are to aid the eye.

In reality, the particles find a way to reduce interaction without statically confining to the central sites, resulting in a more extended one-body profile.

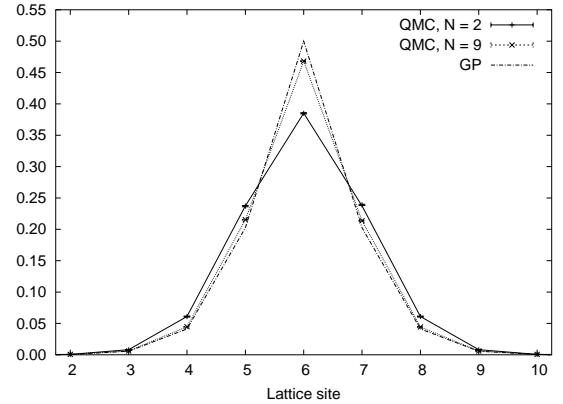


FIG. 5: The normalized density profiles as an illustration of particle correlation effects. Results are for 13-site systems along the GP isoline $U/(N-1) = 2.30t$. The normalized GP curve is identical for any number of particles along this line. QMC results are shown for $N = 2$ and $N = 9$. The QMC results have very small errorbars and are indistinguishable from ED (not shown). The QMC density profiles are more extended, although the interaction energies are lower than GP, as shown in Fig. 4.

B. Comparison with analytic results in 1-D: $a_s < 0$

The problem of an arbitrary number of untrapped bosons interacting with an attractive δ -potential in one dimension can be solved analytically [31], yielding analytic expressions for the total energy and density profile. In this section we carry out QMC and GP calculations and compare our results against these analytic results, on systems of up to 400 bosons. The

Hamiltonian in the continuous real space is

$$\hat{H} = \frac{1}{2} \sum_{i=1}^N \frac{\partial^2}{\partial \mathbf{x}_i^2} + \frac{1}{2} g \sum_{i>j=1}^N (\mathbf{x}_i - \mathbf{x}_j)^2 \quad (52)$$

The interaction constant ($g > 0$) is related to our Hubbard parameters by $g = J^2/t^2$. The ground state of this Hamiltonian is an N -boson bound state. By fixing the center of mass at $\mathbf{x} = 0$, we can eliminate the contribution from its overall motion, which leads to the following analytic expressions for the density profile [32],

$$\rho(\mathbf{x}) = \frac{1}{2} g \sum_{n=1}^N \frac{N!}{(N-n)!} \frac{e^{-g n N}}{(N-n)!} \quad (53)$$

and the total energy,

$$E = -\frac{1}{96} g^2 N^2 \quad (54)$$

In our QMC calculations, we again put the system on a real-space lattice. The lattice size is chosen to be large enough so that discretization errors are comparable to or smaller than statistical errors. As the ground state of the system is a droplet in the absence of the external confining potential, the center of mass can slide in the calculation due to random noise. We therefore need to subtract the center-of-mass motion. Technically, this can be accomplished conveniently in the random walk by treating the system with respect to its center of mass. In Appendix B, we describe our method for this correction, which is applicable in any situation where the center of mass and relative motions need to be separated. In our calculations, the correction affects the kinetic and total energies as well as the density profiles. The results shown below were all obtained with such a correction applied.

We first study a system of 20 particles with $g = 0.154$. Table II shows the energies, and Fig. 6 the density profiles. This is a system where mean-field makes significant errors. Our QMC results are in excellent agreement with the exact results.

TABLE II: Comparison of QMC and GP results to available exact results. The system has 20 particles and $g = 0.154$. A lattice of 1024 sites was used, with $\epsilon = 0.01$ and $b_p = 2.5$.

Type	g.s.energy	$\langle \hat{H} \rangle$	$\langle \hat{H}_{2B} \rangle$	cond.frac.
Analytic result	1.971	-	-	-
QMC	1.964 (8)	2.044 (8)	4.007 (4)	99.76%
GP	1.784	1.776	3.561	100%

We next scan systems with various numbers of particles by following the GP isoline $g(N-1) = 4.0$. The energy per particle is shown as a function of N in Fig. 7, for up to 400 particles. Fig. 8 shows the density profiles for up to 100 particles. Again, the agreement between QMC and exact results is excellent. As the interaction strength g is increased or as N is decreased, mean-field results deviate more and more from the exact results. For example, as we go from $g = 0.01$

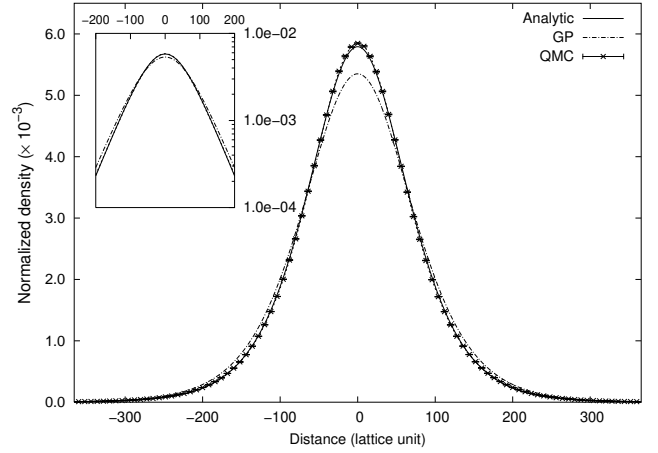


FIG. 6: Comparison of calculated density profiles from QMC and GP with analytical results. The densities are normalized. The QMC errorbars are displayed every five data points to avoid cluttering the plot. The QMC profile is given by the dotted curve. The inset shows the same curves with logarithmic vertical scale, indicating that at large distances the density is exponential.

($N = 400$) to 10 times the strength along the isoline, the systematic error in the GP total energy increases roughly from 0.5% to 5%.

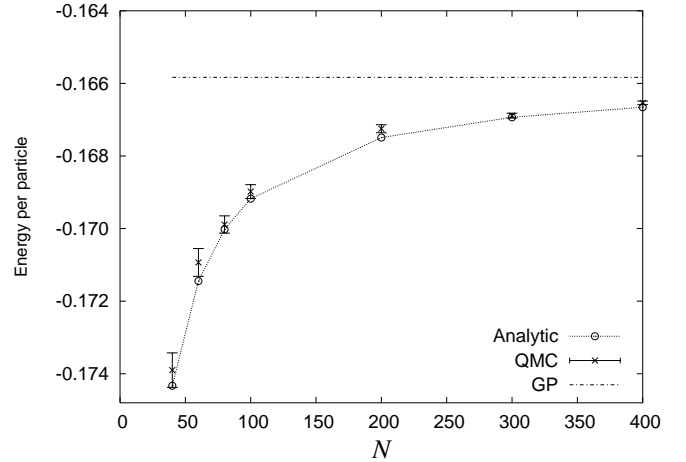


FIG. 7: Comparison of the energy from QMC (crosses) with the exact answer (dotted curve) for different number of particles. Energy per particle is shown along the GP isoline $g(N-1) = 4.0$. The GP result is the flat, dash-dotted line. We use a lattice of 1024 sites, $\epsilon = 0.01$ and $b_p = 4.0$.

We now study the system along a different line, holding the interaction strength g fixed while scanning the number of particles, again up to $N = 400$ particles. Figure 9 shows the behavior of $\langle \hat{H} \rangle / N^3$ for up to 400 particles, with $g = 0.0403$. At large N , the total energy is roughly proportional to N^3 . Compared to Figs. 7 and 8, the interaction strength here is stronger at larger N and weaker at lower N , with the crossover at $N \approx 100$. Most of the calculations are therefore more

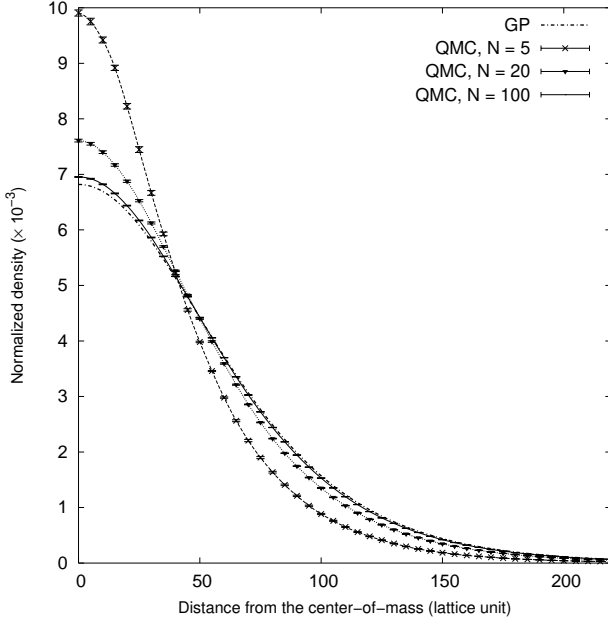


FIG. 8: Comparison of the density profiles from QMC and GP with analytic results. The normalized densities are shown along the GP isoline $\varphi(N=1) = 4.0$ for several N values. The system is the same as that in Fig. 7. The GP density is the same for any N on the isoline, and is given by the dash-dotted line.

challenging numerically. Again QMC was able to completely recover the correlation energy missed by GP. At large N , smaller timesteps were used and more computing was necessary to reduce the statistical errors. (Note that the errorbars appear larger at smaller N in the plot because of the division by N^3 .)

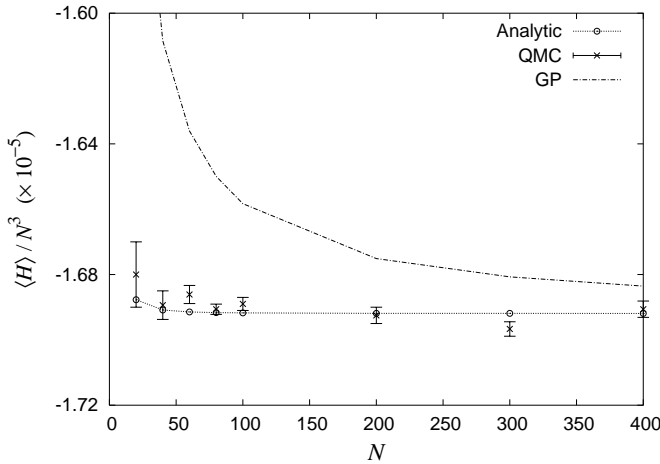


FIG. 9: Comparison of computed ground-state energy for different numbers of particles N . The interaction strength is held constant at $g = 0.0403$. The total energy divided by N^3 is shown as a function of N for QMC, GP and exact calculations. Conservative parameters were used, with $t_{bp} = 4.0$ in all case, and $\epsilon = 0.01$ for $N < 200$ and $\epsilon = 0.005$ otherwise.

C. Comparison with exact diagonalization: $a_s > 0$

We have shown that our new QMC algorithm is exact and works well for a wide range of systems with attractive interactions. If the interaction is repulsive ($a_s > 0$, or equivalently $U > 0$) the one-body propagators resulting from the HS transformation become *complex*, in the form of $\exp(i \frac{U}{2} \mathbf{x}_i \cdot \mathbf{x}_i)$. The same algorithm applies in this case as well. In principle the complex one-body operator only requires a change to the corresponding complex operations. But in practice a serious phase problem occurs, which causes the calculation to lose efficiency rapidly at larger interaction strengths. We discuss this problem and how to control it below. Our initial studies indicate that, for moderate interaction strengths, the algorithm as is remains very efficient and gives accurate results, allowing reliable calculations for parameters corresponding to experimental situations in 3-D.

We benchmark our algorithm in one- and two-dimensional systems with repulsive interactions against exact diagonalization. Table III shows results for a one-dimensional system, with 13 sites and 4 particles. The agreement between QMC and exact result is excellent. Results from GP are also shown. The GP and QMC density profiles have roughly the same size, as evident from the values of $\langle \hat{N}_{\text{trap}} \rangle$. However, GP overestimates the interaction energy because it does not take into account the particle-particle correlation. In the mean field picture, expanding the density profile is the only way to lower the interaction energy, so that the particles overlap less with each other. (Note that $\langle \hat{N}_{\text{trap}} \rangle$ is indeed slightly larger for GP.) In reality, particles can avoid each other more effectively by means of many-body correlation. The QMC correctly recovers this correlation, which lowers the total energy without spreading the density as much as GP does.

TABLE III: Comparison of QMC results against exact diagonalization (ED) and Gross-Pitaveskii (GP) in 1-D. Here we use 13 sites and 4 particles; $t = 2.676$, $U = +1.538$, $\epsilon = 0.3503$; $\epsilon_{bp} = 0.01$ and $\epsilon_{bp} = 2.5$.

Type	g.s.energy	$\langle \hat{H} \rangle$	$\langle \hat{N}_{\text{trap}} \rangle$	$\langle \hat{N}_{2B} \rangle$	cond.frac.
ED	4.24	1.18	1.793	1.269	98.5%
QMC	4.24 (2)	1.18 (2)	1.790 (8)	1.273 (8)	98.6%
GP	4.43	1.03	1.800	1.599	100%

Table IV shows results for bosons in a two-dimensional trap, using a 4×4 lattice. The GP solution also exhibits the same behavior as in the 1-D calculation, in that the density profile is slightly more extended, and the interaction energy is overestimated. As in other cases, the QMC statistical errorbar on the condensate fraction was not computed directly, but we estimate it to be on the last digit.

As mentioned earlier, the only modification necessary to the algorithm in order to treat repulsive interactions ($a_s > 0$) is to allow complex arithmetic. A more serious problem can occur, however. The orbitals and the walker weights become complex numbers. Asymptotically the phase of these weights will be uniformly distributed in the complex plane. The de-

TABLE IV: Comparison of QMC calculations against exact diagonalization (ED) and Gross-Pitaevskii (GP) projection in a 4×4 lattice, with 4 bosons. $t = 0.2534$, $U = +0.3184$, $\mu = 3.700$; $\beta = 0.01$ and $\beta_p = 2.5$.

Type	g.s.energy	$\langle \hat{n} \rangle$	$\langle \hat{n}_{\text{trap}} \rangle$	$\langle \hat{n}_{2B} \rangle$	cond.frac.
ED	6.000	1.818	3.8326	0.350	97.8%
QMC	6.005 (6)	1.817 (2)	3.8325 (2)	0.355 (5)	97.8%
GP	6.067	1.763	3.8359	0.469	100%

nomitors in Eqs. (34) and (40) will be dominated by noise, causing the Monte Carlo sampling efficiency to decay and ultimately destroying the algebraic scaling of QMC. This is the so-called sign or phase problem [19, 22]. In real-space methods this problem is connected to fermions, but here we have a situation where a phase problem appears in the ground state of a bosonic system. Physically, it is easy to see why a phase problem must occur. Our many-body wave function is being represented in IOR, with only one orbital in each walker. With a repulsive interaction, the only way to reflect correlation effects, i.e., particles avoiding each other, is to make the orbitals complex.

As we see below, our algorithm remains efficient and gives accurate results for large systems with scattering lengths corresponding to experimental situations in 3-D. As the interaction strengths become much stronger, the phase problem will ultimately make the approach ineffective. We have done preliminary calculations in which we control the phase problem by applying a phaseless formalism described in Ref. 22. Our results indicate that the systematic errors introduced by the phaseless approximation are small for moderate interaction strengths. We expect to therefore be able to obtain accurate and reliable results for scattering lengths well into the experimental 'strong-interaction' regime achievable by Feshbach resonance.

D. Realistic calculations in three-dimensions

In this section we present some test results on realistic systems of trapped particles in three-dimensions. QMC results were obtained with back-propagation and conservative choices of β and convergence parameters. We expect the QMC results to be exact. We also carry out the corresponding Gross-Pitaevskii calculations, and make comparisons against our exact QMC results.

Table V shows the result of a QMC calculation for 175 particles in a three-dimensional trap. We choose a trap with a characteristic length $a_{ho} = 8546 \text{ \AA}$. The trap was discretized into a $15 \times 15 \times 15$ lattice, in a range that corresponds to about $5 \times a_{ho}$. The scattering length is $a_s = 22.4 \text{ \AA}$. In this regime the GP solution is a good approximation to the exact ground-state wave function. We see that this is indeed the case in Table V. The interaction energy is lowered in the many-body calculation as expected. Interestingly, the external potential energy is lower than in GP. Consistent with this, the

exact density profile is tighter than in GP, as shown in Fig. 10. The trend here appears different from what we observed in small 1-D trapped systems in Fig. 5, but consistent with the large untrapped systems in Fig. 8. We are presently carrying out more calculations to cover a wider range of parameters and study the role of dimensionality.

TABLE V: Comparisons of QMC and GP calculations for 175 particles in a 3-D spherical trap, with $a_s = 22.4 \text{ \AA}$ and $a_{ho} = 8546 \text{ \AA}$. The energies are displayed as per-particle quantities. Both the QMC and GP results are extrapolated to $\beta \rightarrow 0$.

Type	g.s.energy	$\langle \hat{n} \rangle$	$\langle \hat{n}_{\text{trap}} \rangle$	$\langle \hat{n}_{2B} \rangle$	cond.frac.
QMC	16.979 (6)	16.47 (5)	6.54 (1)	6.03 (4)	99.73%
GP	17.115	15.60	6.77	5.25	100%

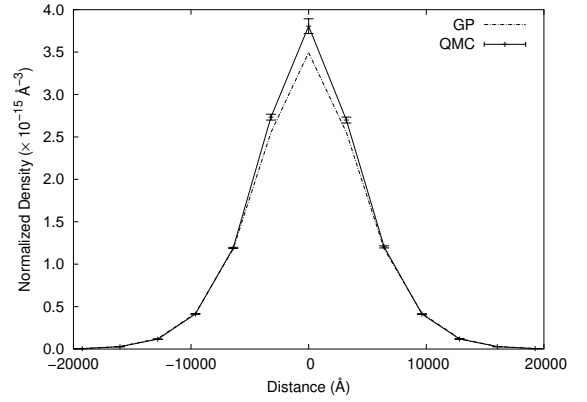


FIG. 10: Comparison of density profiles from the QMC and GP for 175 particles. The system is the same as described in Table V. The QMC profile is more peaked and tighter than GP.

We now turn to bosons with repulsive interactions in three-dimensional trap. We again use a $15 \times 15 \times 15$ lattice, and simulate 100 bosons. We choose a scattering length a_s of 80 \AA . This value is close to the experimental ^{39}K singlet [33] or ^{87}Rb triplet [34] scattering lengths. In Table VI we show the calculated energies and condensate fraction. For this interaction strength, the impact of the phase problem on the statistical error is small, and the QMC calculation is very efficient. The true condensate is, like in the 1-D repulsive case, tighter than that predicted by GP, with lower interaction energy.

TABLE VI: QMC calculation of 100 particles in a three-dimensional trap. A lattice of $15 \times 15 \times 15$ was used. The parameters correspond to $a_{ho} = 8546 \text{ \AA}$ and $a_s = 80 \text{ \AA}$. The quantities displayed are for per particle.

Type	g.s.energy	$\langle \hat{n} \rangle$	$\langle \hat{n}_{\text{trap}} \rangle$	$\langle \hat{n}_{2B} \rangle$	cond.frac.
QMC	24.687 (9)	9.573 (9)	11.933 (5)	3.181 (3)	99.80%
GP	24.922	9.281	12.028	3.612	100%

VI. DISCUSSIONS

A. Connection between QMC and Gross-Pitaevskii projections

The QMC method we have presented allows us to go beyond mean-field and treat many-body effects. On the other hand, it has a deep connection with the GP mean-field approach. Our approach uses an HS transformation which leads to integrals of single-particle operators over auxiliary-fields. The mean-field solution can be regarded as the leading term in the stationary-phase asymptotic expansion of the exact solution [35]. Our method evaluates this exact solution, which is in the form of many-dimensional integrals, by Monte Carlo. In this section we further comment on the formal connection between our importance-sampled QMC and the GP as done by projection (the second of the two GP methods discussed in subsection IV C).

Let us reconsider the two-body propagator in the modified AF transformation Eq. (25). Let us suppose that we are now taking our first Monte Carlo step, where our walker is j_i , and we will also use the same wave function as j_T . Following the discussion of the optimal choice of \underline{x} in the same section, III B, we know that $\underline{x} = 0$ is a stationary point with the choice

$$\underline{x}_i = \frac{P}{v_i} \frac{P}{h} \frac{j_{i,j_i}}{h j_i} : \quad (55)$$

We can approximate the integral in Eq. (25) by the value of the integrand at $\underline{x} = 0$, which can be justified in the limit of small β . More explicitly, as $\beta \rightarrow 0$, the Gaussian function becomes the most rapidly varying term in the integrand. To exhibit the asymptotic behavior of this integral, we change the integration variable to $\underline{y} = \underline{x}$, so that the large parameter $1/\beta$ appears in the Gaussian's exponent:

$$e^{\frac{1}{2} \underline{\phi}^2} = e^{-\frac{1}{2} \underline{v}^2 \underline{v} \underline{\phi}} \int_1^Z \frac{1}{dy} \frac{e^{-\frac{y^2-2}{2}}}{2} e^{y(\underline{\phi} \underline{v})} :$$

The dominant contribution to the integral comes from the maximum of the Gaussian function at $y = 0$. The asymptotic leading term of the importance-sampled many-body propagator is therefore:

$$e^{-K \frac{P}{v_i} \underline{v}_i \underline{\phi}_i + \frac{1}{2} \frac{P}{v_i} \underline{v}_i^2} ; \quad (56)$$

where \hat{K} is the one-body term in the original Hamiltonian. Under this approximation, our random walk becomes deterministic, needing only one walker. If for the next step we use the updated wave function j_0 to evaluate the new $f v_i g$ in Eq. (55), we obtain a self-consistent projection with one-body propagators. In fact, the one-body Hamiltonian in the exponent of Eq. (56) is precisely the mean-field Hamiltonian. For example, for Bose-Hubbard model the last two terms in the exponent lead to the GP mean-field potential

$$U \sum_i n_i \hat{n}_i + \frac{1}{2} n_i^2 : \quad (57)$$

Apart from the factor $(N-1)/N$ which approaches unity in the limit of large N , we have recovered the GP propagator.

The projection with Eq. (56) lowers the variational energy for any initial j_i and is stationary when j_i is the GP solution. This is why GP is the best variational wave function that has the form of a single permanent, and hence a reasonable trial wave function to use for most of our QMC calculations.

It is also clear from the discussion above that the importance sampling formalism allows us to have an optimal form of HS transformation, in that the HS propagator $e^{y(\underline{\phi} \underline{v})}$ involves only the difference $\underline{\phi} \underline{v}$. In other words, although in Eq. (7) we write the decomposition for the bare interaction term, the importance sampling transformation effectively introduces a mean-field background based on the trial wave function and allows the HS to deal with only a residual quadratic interaction term, $(\underline{\phi} \underline{v})^2$.

To summarize, our QMC method reduces to GP if we evaluate the many-body propagator by the stationary-point approximation, using only the centroid of the Gaussian. The full method evaluates the many-dimensional integral over auxiliary-fields exactly by Monte Carlo. It captures the interaction and correlation effects with a stochastic, coherent ensemble of mean-field solutions. The structure of the calculation can be viewed as a superposition of the GP projections that we have described. Our method therefore provides a way to systematically improve upon GP while using the same framework.

B. Computing

Because of the structure of QMC as a superposition of GP projections, our method scales gracefully with system size. As discussed in Sec. IV B, the bulk of our method scales as $O(M \log M)$, with the significant speedup from using Fast Fourier transform. For example, the QMC calculation shown in Table VI required less than 8 hours on a single Alpha EV67 processor. The 1024-sites QMC calculation shown in Table II took about four hours to get good statistics, with very conservative choices of β and other convergence parameters. It required about 1.3 gigabytes of memory, largely because of back-propagation path recording. In contrast, treated fully, the latter problem would mean the diagonalization of a sparse, Hermitian matrix containing $(8 \cdot 10^4)^2$ elements. Although this can be reduced by exploiting symmetries, exact diagonalization of this problem is clearly not within reach with computing capabilities in the foreseeable future.

We typically use hundreds of walkers in our calculation. The stochastic nature of QMC means the number of walkers fluctuates due to branching and killing of walkers with very large and very small weights (see subsection III). The population therefore must be controlled to ensure that it does not grow or decay too much, and that the walker weights have a reasonable distribution. Our method to control the population is similar to that discussed in Ref. 25.

We comment on the effect of the number of particles, N , on scaling. Because of the use of IOR, the number of particles does not enter in the propagation. It would then seem as though the algorithm might have a super-scaling in N . This is not true, of course, since the projector $e^{-\hat{H}}$ depends on

N . For example, the shift v_1 has a factor of N in front (see Appendix A), and the local energy scales with N . As a result, a smaller time-step must be used for larger N . The above argument suggests a linear reduction in τ as N is increased, which we have used as a rough guideline in our calculations to select the range of τ to use. Extrapolations with separate calculations using different τ values are then carried out.

C. Conclusion and Outlook

In conclusion, we have presented a new auxiliary-field QMC algorithm for obtaining the many-body ground state of bosonic systems. The method, which is based upon the field-theoretical framework and is essentially exact, provides a means to treat interactions more accurately in many-body systems. Our method shares the same framework with the GP approach, but captures interaction and correlation effects with a stochastic ensemble of mean-field solutions. We have illustrated our method in trapped and untrapped boson atomic gases in 1-, 2-, and 3-dimensions, using a real-space grid as single-particle basis which leads to a Bose-Hubbard model for these systems. We have demonstrated its ability to obtain exact ground-state properties. We have also carried out the GP mean-field calculations and compared the predictions with our exact QMC results. Our method is capable of handling large systems, thus providing the possibility to simulate system sizes relevant to experimental situations. We expect the method to complement GP and other approaches, and become a useful numerical and theoretical tool for studying trapped atomic bosons, especially with the growing ability to tune the interaction strengths experimentally and reach more strongly interacting regimes.

From the methodological point of view, more work remains to be done with the repulsive case to deal with the phase problem. We have shown that our method as it stands can be very useful for moderate interaction strengths. For stronger interactions, our preliminary study indicates that the phaseless approximation [22], which eliminates the phase problem but introduces a systematic error, is very accurate for scattering lengths well into the Feshbach resonance regime. We are currently examining this more systematically to quantify the extent of the bias. Because of the simplicity of these bosonic systems compared to electronic systems, they provide an ideal testbed, where for small sizes the problem is readily solved by exact diagonalization.

A variety of applications are possible. The ground state of the Bose-Einstein condensates with both attractive and repulsive interatomic interactions can be studied for various interaction strengths, including the strongly interacting regime reached by Feshbach resonance. They can also be studied in different dimensions and under different conditions. In particular, it would seem straightforward to generalize our present framework to study rotations and vortices, since we are already dealing with complex propagators and wave functions in the repulsive case. In addition, it will be interesting to treat boson-fermion mixtures with our approach. As mentioned, the auxiliary-field method is already widely used to

treat strongly interacting fermion systems.

Acknowledgments

We thank D. M. Ceperley and H. Krakauer for stimulating discussions. Financial support from NSF (grant DMR-9734041), ONR (grant N00014-97-1-0049), and the Research Corporation is gratefully acknowledged. SZ expresses his gratitude to Prof.'s Ceperley and Richard Martin for their hospitality during a sabbatical visit, where part of the work was carried out. We also thank the Center of Piezoelectric by Design (CPD), where part of our computing was performed.

APPENDIX A: IDENTICAL-ORBITAL REPRESENTATION

In this appendix we show that the matrix representation of an N -boson wave function in AFQMC can be made particularly simple. In fermion calculations, we must use an $M \times N$ matrix to represent a determinant, because the orbitals must be mutually orthogonal. In the boson case, however, this restriction is absent. The most general form of a many boson permanent is expensive to compute, having complexity of $O(N!M^N)$. But we can choose to make all the orbitals identical. In matrix language, we will have only an M -row column vector. We will term this representation *identical-orbital representation*—IOR. Each many-boson wave function in IOR has the form of a GP mean-field solution. Two conditions are necessary for this choice to be viable in the QMC: that an initial trial wave function of this form is allowed and that successive projections preserve the form. The only requirement for the former to hold is that the wave function in IOR not be orthogonal to the true many-body ground state, and it is straightforward to show that Eq. (12) holds for a j in this form. More complex wave functions can always be generated by a linear combination of such wave functions. In fact, this is what we accomplish through our Monte Carlo simulation.

In operator language, a single N -boson wave function j is given by

$$|j\rangle = \frac{1}{N!} \sum_{\mathbf{z}} \hat{c}^{\dagger}_{\mathbf{z}} \hat{c}_{\mathbf{z}}^N |0\rangle = \frac{1}{N!} \sum_{\mathbf{z}} \hat{c}_{\mathbf{z}}^N |0\rangle;$$

where $\hat{c}_{\mathbf{z}}^{\dagger} = \sum_{\mathbf{r}} \hat{c}_{\mathbf{r}}^{\dagger} \phi_{\mathbf{z}}(\mathbf{r})$. In matrix form, $|j\rangle$ would be $M \times 1$ matrix whose columns are identical. The overlap of two such wave functions is given by

$$\langle j | i \rangle = \frac{1}{N!} \sum_{\mathbf{z}} \langle \mathbf{z} | \hat{c}_{\mathbf{z}}^N | 0 \rangle \langle 0 | \hat{c}_{\mathbf{z}}^N | i \rangle = N! (\langle \mathbf{z} | \hat{c}_{\mathbf{z}} | i \rangle)^N;$$

where the bold-phased symbols $\hat{c}_{\mathbf{z}}$ and $\langle \mathbf{z} |$ represent the single-column vectors for $\hat{c}_{\mathbf{z}}$ and $\langle \mathbf{z} |$, respectively. Similarly, for any one-body operator \hat{A} ,

$$\langle j | \hat{A} | i \rangle = N! N (\langle \mathbf{z} | \hat{A} | \mathbf{z} \rangle)^{N-1}; \quad (\text{A1})$$

where A is the matrix for \hat{A} . The matrix element of a quartic (two-body) operator is given by:

$$\langle \mathbf{r} | \hat{A} | \mathbf{r}' \rangle = \sum_{i,j} A_{ij} \psi_i(\mathbf{r}) \psi_j(\mathbf{r}') \quad (A2)$$

APPENDIX B: DROPLET CENTER-OF-MASS CORRECTION

1. Correcting the density broadening

To handle the droplet system given by the translationally invariant Hamiltonian in Eq. (52), an extra ingredient is necessary in addition to the “basic” QMC algorithm that we have described. In a deterministic calculation, for example in GP, the motion of the center-of-mass (CM) can be simply eliminated by fixing it at the origin, as in Eq. (53). In the QMC calculation, however, the orbitals fluctuate as they are propagated by $\hat{E}(\mathbf{x})$, where the random fields \mathbf{x} are drawn from a Gaussian probability density. Random noise will inevitably cause the CM of the system to slide, undergoing a free diffusion whose average position is the origin.

Left unchecked, this spurious CM motion will lead to an artificial broadening of the density profile. To correct for it in the density profile, we could simply shift the CM of every walker back to the origin. However, the importance-sampled propagator involves ratios of overlaps with the trial wave function $\psi_T(\mathbf{r})$, which would have to be corrected in the random walk whenever a shift is made.

Instead our solution to this diffusive motion is to let the trial wave function slide along with the walkers. In other words, we rewrite the kinetic energy operator as

$$\hat{T} = \hat{T}_{\text{cm}} + \hat{T}^0; \quad (B1)$$

where \hat{T}_{cm} represents the CM kinetic energy, and \hat{T}^0 the internal kinetic energy in the CM frame. The total Hamiltonian is given by

$$\hat{H} = \hat{T}_{\text{cm}} + \hat{T}^0 + \hat{V} = \hat{T}_{\text{cm}} + \hat{H}^0; \quad (B2)$$

The quantities that we wish to compute are governed by the “internal” Hamiltonian \hat{H}^0 . Since \hat{V} involves only relative coordinates among the particles, it commutes with \hat{T}_{cm} ; or more generally,

$$[\hat{T}_{\text{cm}}, \hat{H}^0] = 0; \quad (B3)$$

In this way, the importance-sampled QMC propagation is determined by \hat{H}^0 . The motion of the CM in each walker is a separate free diffusion which is governed by \hat{T}_{cm} . In the random-walk process, we are now free to correct for the CM motion by shifting the walkers back to the origin whenever necessary. For consistency, this correction must be applied both in the normal random walk and in the back-propagation phase.

2. Separating the center-of-mass kinetic energy

The moving trial wave function, however, poses a problem for the calculation of the kinetic energy. Now the orbitals are

free to slide, and the diffusive motion of the orbital’s CM is no longer suppressed in the LAB frame. When we use the usual \hat{T} -term in the Hamiltonian in Eq. (43) to compute the kinetic energy, we obtain the total $\langle \hat{T} \rangle$, in which $\langle \hat{T}_{\text{cm}} \rangle$ and the desired $\langle \hat{T}^0 \rangle$ are mixed. This leads to a spurious increase in the estimate of the kinetic energy and consequently the total energy. For example, the *uncorrected* ground-state energy for the system shown in Table II would be $-1.387(2)$ with $\langle \hat{T} \rangle = -2.092(3)$; thus the total energy is overestimated by 0.08 due to the contribution from $\langle \hat{T}_{\text{cm}} \rangle$. Since we know the nature of the CM motion, it is fairly straightforward to extract $\langle \hat{T}_{\text{cm}} \rangle$ and explicitly subtract it from the kinetic and total energy estimates. Allowing the droplet to freely slide in the calculation is equivalent to having a spurious “propagator” $e^{-\hat{T}_{\text{cm}} \tau}$, whose effect on the wave function for the CM is described by the diffusion equation

$$\frac{\partial \psi_{\text{cm}}(\mathbf{R}; \tau)}{\partial \tau} = \hat{T}_{\text{cm}} \psi_{\text{cm}}(\mathbf{R}; \tau);$$

It is a well known property of such a diffusion process that the averaged squared distance $\langle |\mathbf{R}^2(\tau)| \rangle$ grows linearly with the (imaginary) time τ :

$$\langle |\mathbf{R}^2(\tau)| \rangle = b \tau;$$

We can obtain b by recording the quantity $\langle |\mathbf{R}^2(\tau)| \rangle$ for a period of time in the QMC simulation. The constant b is linearly proportional to $\langle \hat{T}_{\text{cm}} \rangle$. More specifically, the center-of-mass Hubbard hopping parameter t_{cm} can be extracted from b :

$$t_{\text{cm}} = b/2; \quad (B4)$$

This gives us the correct kinetic and total energies without the spurious center-of-mass motion:

$$\langle \hat{T}^0 \rangle = \langle \hat{T} \rangle - \frac{t_{\text{cm}}}{\tau} \langle \hat{T} \rangle; \quad (B5a)$$

$$\langle \hat{H}^0 \rangle = \langle \hat{H} \rangle - \langle \hat{T}_{\text{cm}} \rangle; \quad (B5b)$$

To conclude, there are two necessary modifications in the QMC algorithm in order to treat quantum droplets which are not confined:

1. We let the trial wave function effectively “follow” the QMC orbitals, by defining its CM with that of each QMC orbital.
2. For each orbital, we keep track and accumulate all the applied CM shifts in order to estimate $\langle |\mathbf{R}^2(\tau)| \rangle$. This gives us the fraction of CM kinetic energy through the constant t_{cm} .

These modifications in the QMC allows us to obtain the correct density profile and energies of a translationally-invariant Hamiltonian.

-
- [1] M. H. Anderson, J. R. Ensher, M. R. Matthews, C. E. Wieman, and E. A. Cornell, *Science* **269**, 198 (1995).
 - [2] F. Dalfovo, S. Giorgini, L. P. Pitaevskii, and S. Stringari, *Rev. Mod. Phys.* **71**, 463 (1999).
 - [3] A. J. Leggett, *Rev. Mod. Phys.* **73**, 307 (2001).
 - [4] S. L. Cornish, N. R. Claussen, J. L. Roberts, E. A. Cornell, and C. E. Wieman, *Phys. Rev. Lett.* **85**, 1795 (2000).
 - [5] W. M. C. Foulkes, L. Mitas, R. J. Needs, and G. Rajagopal, *Rev. Mod. Phys.* **73**, 33 (2001), and also the references therein.
 - [6] D. M. Ceperley, *Rev. Mod. Phys.* **67**, 279 (1995), and also the references therein.
 - [7] W. Krauth, *Phys. Rev. Lett.* **77**, 3695 (1996).
 - [8] P. Grüter, D. Ceperley, and F. Laloë, *Phys. Rev. Lett.* **79**, 3549 (1997).
 - [9] M. Holzmann and W. Krauth, *Phys. Rev. Lett.* **83**, 2687 (1999).
 - [10] J. L. DuBois and H. R. Glyde, *Phys. Rev. A* **63**, 023602 (2001).
 - [11] J. L. DuBois and H. R. Glyde, *Phys. Rev. A* **68**, 033602 (2003).
 - [12] M. Ulmke and R. T. Scalettar, *Phys. Rev. B* **61**, 9607 (2000).
 - [13] R. Blankenbecler, D. J. Scalapino, and R. L. Sugar, *Phys. Rev. D* **24**, 2278 (1981).
 - [14] G. Sugiyama and S. E. Koonin, *Ann. Phys.* **168**, 1 (1986).
 - [15] J. Hubbard, *Phys. Rev. Lett.* **3**, 77 (1959).
 - [16] R. D. Stratonovich, *Dokl. Akad. Nauk. SSSR* **115**, 1907 (1957).
 - [17] J. E. Hirsch, *Phys. Rev. B* **28**, 4059 (1983).
 - [18] S. R. White, D. J. Scalapino, R. L. Sugar, E. Y. Loh, J. E. Gubernatis, and R. T. Scalettar, *Phys. Rev. B* **40**, 506 (1989).
 - [19] S. Zhang, J. Carlson, and J. E. Gubernatis, *Phys. Rev. B* **55**, 7464 (1997).
 - [20] D. J. Dean and S. E. Koonin, *Phys. Rev. C* **60**, 054306 (1999).
 - [21] S. Fantoni, A. Sarsa, and K. E. Schmidt, *Phys. Rev. Lett.* **87**, 181101 (2001).
 - [22] S. Zhang and H. Krakauer, *Phys. Rev. Lett.* **90**, 136401 (2003).
 - [23] H. F. Trotter, *Proc. Am. Math. Soc.* **10**, 545 (1959).
 - [24] M. Suzuki, *Commun. Math. Phys.* **51**, 183 (1976).
 - [25] S. Zhang, in *Theoretical Methods for Strongly Correlated Electrons*, edited by D. Sénéchal, A.-M. Tremblay, and C. Bourbonnais (Springer, New York, 2003), CRM Series in Mathematical Physics, pp. 39–74.
 - [26] D. R. Hamann and S. B. Fahy, *Phys. Rev. B* **41**, 11352 (1990).
 - [27] E. P. Gross, *Nuovo Cimento* **20**, 454 (1961).
 - [28] E. P. Gross, *J. Math. Phys.* **4**, 195 (1963).
 - [29] L. P. Pitaevskii, *Sov. Phys.-JETP* **13**, 451 (1961).
 - [30] P. A. Ruprecht, M. J. Holland, K. Burnett, and M. Edwards, *Phys. Rev. A* **51**, 4704 (1995).
 - [31] J. B. McGuire, *J. Math. Phys.* **5**, 622 (1964).
 - [32] F. Calogero and A. Degasperis, *Phys. Rev. A* **11**, 265 (1975), and also the references therein.
 - [33] J. L. Bohn, J. P. Burke, C. H. Greene, H. Wang, P. L. Gould, and W. C. Stwalley, *Phys. Rev. A* **59**, 3660 (1999).
 - [34] J. Weiner, V. S. Bagnato, S. Zilio, and P. S. Julienne, *Rev. Mod. Phys.* **71**, 1 (1999).
 - [35] J. W. Negele and H. Orland, *Quantum Many-Particle Systems*, Advanced Book Classics (Perseus Books, Reading, Massachusetts, 1998).